CFD Investigations of Wave Interaction with a Pair of Large Tandem Cylinders

Arun Kamath[1], Mayilvahanan Alagan Chella, Hans Bihs, Øivind A. Arntsen

Department of Civil and Transport Engineering, Norwegian University of Science and Technology, 7491 Trondheim, Norway

Abstract

Wave forces and the flow field around cylinders placed in a periodic wave field are investigated with a numerical model using the Reynolds-averaged Navier-Stokes equations. The numerical model is validated by simulating the wave interaction with a single cylinder and comparing the numerical results with experimental data from a large scale experiment. Then, the wave interaction with a single large cylinder and a pair of large cylinders placed in tandem for different incident wave steepnesses is studied. The numerically calculated forces are compared with predictions from potential theory. The numerical results are seen to match the predictions at low incident wave steepness but differ at higher incident wave steepnesses. The wave diffraction pattern around the tandem cylinders for waves of low and high steepness is investigated and the evolution of a strong diffraction pattern is seen in the case of high steepness waves, which results in the difference between the wave forces predicted by potential theory and the numerical model at higher steepnesses.

Keywords: wave forces, wave interaction, vertical cylinders, numerical wave tank, CFD

[1]Corresponding Author, Email: arun.kamath@ntnu.no, Ph: (+47) 73 59 46 40, Fax: (+47) 73 59 70 21

1. Introduction

Circular cylindrical structures are commonly used in the support structures of offshore wind turbines, oil and gas platforms, offshore mooring dolphins in deep and intermediate waters and nearshore coastal structures. Understanding the interaction of waves with these structures is important for the accurate prediction of the hydrodynamic loads on them. Moreover, the interaction of waves with large cylindrical structures always modifies the characteristics of the incident wave field and influences the wave induced processes of wave radiation and diffraction. The modified kinematics of the flow field changes the flow processes such as the wave run-up, reflection and transmission. In the case of a circular cylinder, the contribution of drag and inertia forces to the total forces is determined by the KC number and the diffraction parameter. When the diffraction parameter, which is the ratio of the cylinder diameter (D) to the incident wavelength (L), is greater than 0.2 ($D/L > 0.2$) and the KC number is smaller than 2, the flow is inertia dominated and wave diffraction effects are important (Isaacson, 1979). Lower-order solutions can be obtained with analytical formulations based on potential theory by assuming the fluid is inviscid, the flow irrotational and the wave amplitude small compared to the diameter of the cylinder. The methods based on potential theory are limited by these assumptions, when the incident wave is steep. The importance of non-linear interactions arising from diffracted waves and the viscous effects in an unseparated flow regime have to be investigated by accounting for these phenomena and comparing the results with predictions from potential theory.

MacCamy and Fuchs (1954) derived an equation using linear potential theory to obtain the first-order wave force on a single large cylinder using the wave diffraction potential. This equation is commonly used to determine wave forces on a single large cylinder exposed to regular waves. Chakrabarti and Tam (1973) carried out experimental studies on large cylinders exposed to small amplitude waves and found good agreement with predictions from linear potential theory. Some studies proposed certain methods to evaluate higher order forces using potential theory (Lighthill (1979), Molin (1979)), but had difficulties in obtaining convergent solutions.

In a diffraction regime, the incident wave train is affected by its interaction with the cylinder and its effects are seen even outside the immediate vicinity of the cylinder. This results in a complex hydrodynamic problem when groups of large cylinders are placed in a wave field. Ohkusu (1974) proposed an iterative method to evaluate successive water wave scattering by floating bodies, based on the work by Twersky (1952) for electromagnetic and acoustic waves. The velocity potential functions used in this approach become harder to work with as the number of cylinders is increased. Spring and Monkmeyer (1974) proposed a method where all the boundary conditions are enforced at once and the wave forces are determined by solving a set of linear equations. Linton and Evans (1990) improved the method by Spring and Monkmeyer (1974) and proposed a method with a simplified expression for the velocity potential to obtain the maximum first-order force, the mean second-order force on the cylinder and to calculate the free surface amplitudes for equally spaced identical cylinders. Using this analytical method, it is possible to evaluate the amplitude of the wave forces on cylinders placed in a group and to determine the maximum variation of the free surface around the cylinders.

The limitation of analytical formulae based on potential theory is that they have to be modified to deal with different scenarios, for example, to study structures of different geometries, to study non-linear wave-wave and wave-body interactions due to waves of high steepnesses. Numerical modeling based on boundary integral equations (Ferrant (1995), Boo (2002), Song et al. (2010)) have the same limitations as potential theory, on which they are based. On the other hand, Computational Fluid Dynamics (CFD) modeling provides an immense amount of detail regarding the wave hydrodynamics by representing most of the wave physics with few assumptions. CFD modeling of wave interaction with large cylinders placed close to each other can provide more insight into the physical processes, such as the effect of wave diffraction on neighboring objects including the wave elevation, wave forces, water particle velocities, the influence of the center-to-center distance and the incident wave steepness. The scale and geometries considered in studies using a CFD model may not be directly applicable to determining the hydrodynamic loads on an offshore structure, but the validation of such a model provide the first step towards establishing such methods to an eventual application to larger and more complicated problems, with realistic geometries and scales in the future, since full scale data and field observations are generally lacking. Another application is to extend the studies to random wave forces Boccotti et al. (2012) after establishing the numerical model for regular waves in this study. The validated numerical model can be used to gain further insight into the applicability of the Morison equation in the case of random waves and build upon the knowledge gained from the field experiments in recent literature Boccotti et al. (2013).

In this study, the open source CFD model, REEF3D (Alagan Chella et al., 2015) is used to analyse wave interaction with bottom-fixed vertical cylinders in a 3D numerical wave tank. The paper presents studies with a large number of simulations investigating the changes in the wave hydrodynamics with small incremental changes in parameters using CFD simulations. The model is validated by comparing the computed wave forces on a single cylinder, free surface elevations around the cylinder and the water particle velocities with the experimental data from the large-scale experiments carried out at the Large Wave Flume (GWK) in Hannover, Germany by Mo et al. (2007). Then, the wave forces on a single cylinder and on a pair of tandem cylinders for different wave steepnesses and center-to-center distances is calculated in 108 numerical simulations. The wave forces on a single cylinder due to waves of different steepnesses are studied, along with the wave elevation around the cylinder. The wave forces experienced by a pair of tandem cylinders with different center-to-center distances and different incident wave steepnesses are evaluated. A total of 96 simulations are carried out to investigate the change in the wave forces with respect to the center-to-center distance and the wave steepness. The wave elevation in the vicinity of the cylinders is studied to gain more knowledge about the wave propagation and the evolution of wave diffraction patterns between the neighboring cylinders. In addition, the analytical formula proposed by Linton and Evans (1990) is used to compare the wave forces on the tandem cylinders for low wave steepnesses where linear potential theory is valid.

2. Numerical Model

2.1. Governing equations

REEF3D uses the incompressible Reynolds-averaged Navier-Stokes (RANS) equations together with the continuity equation to solve the fluid flow problem:

$$\frac{\partial u_i}{\partial x_i} = 0 \tag{1}$$

$$\frac{\partial u_i}{\partial t} + u_j \frac{\partial u_i}{\partial x_j} = -\frac{1}{\rho}\frac{\partial p}{\partial x_i} + \frac{\partial}{\partial x_j}\left[(\nu + \nu_t)\left(\frac{\partial u_i}{\partial x_j} + \frac{\partial u_j}{\partial x_i}\right)\right] + g_i \tag{2}$$

where u is the time averaged velocity, ρ is the density of the fluid, p is the pressure, ν is the kinematic viscosity, ν_t is the eddy viscosity and g the acceleration due to gravity.

The pressure is determined using the projection method (Chorin, 1968) and the resulting Poisson equation is solved with a preconditioned BiCGStab solver (van der Vorst, 1992). Turbulence modeling is carried out using the two equation k-ω model proposed by Wilcox (1994). The strain in the flow due to the waves leads to unphysical overproduction of turbulence in the wave tank. To avoid this, eddy viscosity limiters are used as shown by Durbin (2009). Also, the strain due to the large difference in density at the interface between air and water causes an overproduction of turbulence at the interface. This is avoided by free surface turbulence damping around the interface as shown by Naot and Rodi (1982). The damping is carried out only around the interface using the Dirac delta function. REEF3D is fully parallelised using the domain decomposition strategy and MPI (Message Passing Interface).

2.2. Free Surface

The free surface is determined with the level set method. The zero level set of a signed distance function $\phi(\vec{x},t)$ is used to represent the interface between air and water (Osher and Sethian, 1988). Moving away from the interface, the level set function gives the shortest distance from the interface. The sign of the function distinguishes between the two fluids across the interface as shown in Eq. (3):

$$\phi(\vec{x},t)\begin{cases} >0 & if\ \vec{x}\ is\ in\ phase\ 1 \\ =0 & if\ \vec{x}\ is\ at\ the\ interface \\ <0 & if\ \vec{x}\ is\ in\ phase\ 2 \end{cases} \tag{3}$$

The level set function is moved under the influence of an external velocity field u_j with the convection equation in Eq. (4):

$$\frac{\partial \phi}{\partial t} + u_j \frac{\partial \phi}{\partial x_j} = 0 \tag{4}$$

The level set function loses its signed distance property on convection and is reinitialised after every iteration using a partial differential equation based reinitialisation procedure by Peng et al. (1999) to regain its signed distance property.

2.3. Discretization schemes

The fifth-order conservative finite difference Weighted Essentially Non-Oscillatory (WENO) scheme proposed by Jiang and Shu (1996) is applied for the discretization of the convective terms of the RANS equation. The level set function, turbulent kinetic energy and the specific turbulent dissipation rate are discretised using the Hamilton-Jacobi formulation of the WENO scheme by Jiang and Peng (2000). The WENO scheme is a minimum third-order accurate and numerically stable even in the presence of large gradients. Time advancement for the momentum and level set equations is carried out using a Total Variation Diminishing (TVD) third-order Runge-Kutta explicit time scheme proposed by Shu and Osher (1988). Adaptive time stepping is employed to satisfy the CFL criterion based on the maximum velocity in the domain. This ensures numerical stability throughout the simulation with an optimal value of time step size. A first-order scheme is utilised for the time advancement of the turbulent kinetic energy and the specific turbulent dissipation, as these variables are mostly source term driven with a low influence of the convective terms. Diffusion terms of the velocities are also subjected to implicit treatment in order to remove the diffusion terms from the CFL criterion. The convergence studies for the simulations are then just carried out for the grid size to determine the accuracy of the results, since the adaptive time stepping approach determines the optimal time step required to maintain the numerical stability. As an example, in the case of non-breaking wave interaction with a vertical cylinder presented in this study, time steps are smaller, about 0.002 s during the first few seconds of the simulation as the waves are introduced into the wave tank and then increase to about 0.004 s as the periodic waves are established in the tank. In this way, the adaptive time stepping approach determines the optimal time step, reducing the cost of the simulation and avoiding numerical instability in a simulation which could occur with a fixed time step approach.

The numerical model uses a uniform Cartesian grid for the spatial discretization together with the Immersed Boundary Method (IBM) to represent the irregular boundaries in the domain. Berthelsen and Faltinsen (2008) developed the local directional ghost cell IBM to extend the solution smoothly in the same direction as the discretization, which is adapted to three dimensions in the current model.

2.4. Numerical wave tank

The numerical wave tank uses the relaxation method (Larsen and Dancy, 1983) for wave generation and absorption. This method requires a certain length of the wave tank to be reserved as wave generation and absorption zones. Relaxation functions are used to moderate the velocity and the free surface using a wave theory in the relaxation zones with Eq. (5):

$$\begin{aligned} u_{relaxed} &= \Gamma(x) u_{analytical} + (1 - \Gamma(x)) u_{computational} \\ \phi_{relaxed} &= \Gamma(x) \phi_{analytical} + (1 - \Gamma(x)) \phi_{computational} \end{aligned} \tag{5}$$

where $\Gamma(x)$ is the relaxation function and $x \in [0, 1]$ is the x-coordinate scaled to the length of the relaxation zone. The relaxation function proposed by Jacobsen et al. (2011), shown in Eq. (6) is used in the numerical model.

$$\Gamma(x) = 1 - \frac{e^{x^{3.5}} - 1}{e - 1} \tag{6}$$

The wave theory for moderating the numerical values is chosen according to the wave steepness and the water depth in the simulation. Typically, the wave generation zone is one wavelength long and the absorption zone is two wavelengths long. In the wave generation zone, the computational values of velocity and free surface are raised to the analytical values prescribed by wave theory. The generation zone releases waves into the working zone of the tank. The objects to be studied are placed in the working zone of the tank. The relaxation function in the generation zone also absorbs reflections from structures in the wave tank and prevents them from affecting wave generation. At the end of the tank, the wave enters the numerical beach. Here, the computational values of velocity and free surface are reduced to zero in a smooth manner. This simulates the effect of a beach where the wave energy is removed from the wave tank.

3. Calculation of Wave Forces

3.1. Numerical evaluation of wave forces

The numerical model evaluates the wave force F on an object as the integral of the pressure p and the surface normal component of the viscous shear stress tensor τ on the object according to Eq. (7):

$$F = \int_{\Omega} (-\mathbf{n}p + \mathbf{n} \cdot \tau) d\Omega \tag{7}$$

where $\mathbf{n}$ is the unit normal vector pointing into the fluid and Ω is the surface of the object.

This is readily accomplished by the numerical model as the values for pressure and shear stress are available at every point in the domain at any given time of the simulation.

3.2. Analytical formulae for wave forces

Potential theory is used to obtain the wave diffraction potential and calculate the force on a single cylinder using the equation presented by MacCamy and Fuchs (1954), shown in Eq. (8):

$$|F| = \left| \frac{4\rho g i a \ tanh(kd)}{k^2 H_1'(kr)} \right| \tag{8}$$

where $i = \sqrt{-1}$, a is the incident wave amplitude, $k = 2\pi/L$ the wave number, d the water depth and H_1' the first derivative of the Hankel function of the first kind and r the radius of the cylinder.

An extension of the diffraction theory proposed by Linton and Evans (1990) to calculate wave forces on multiple cylinders placed in proximity is presented in Eq. (9):

$$A_m^l + \sum_{\substack{j=1 \\ \neq l}}^{N} \sum_{n=-M}^{M} A_j^n Z_n^j e^{i(n-m)\alpha_{jl}} H_{n-m}(kR_{jl}) = -I_l e^{im(\frac{\pi}{2}-\beta)}$$

$$l = 1, \ldots, N, \ m = -M, \ldots, M. \tag{9}$$

where, M is the order of the solution, N is the number of cylinders, I is the incident wave potential, β is the angle of wave propagation with respect to the x-axis, H is the Hankel function of the first kind, R_{jl} is the length of the line joining the centers of the jth and the lth cylinder, α_{jk} is the angle between the x-axis and the line joining the centers of the cylinders and $Z = J'(kr_j)/H'(kr_j)$, where J is the Bessel function of the first kind. The unknown coefficients A are to be evaluated. This results in a set of $N(2M+1)$ equations. Linton and Evans (1990) suggest that a value of $M = 6$ provides sufficiently accurate solutions. So, $M = 6$ is used in the equations to obtain the analytical prediction of wave forces in this study.

The unknown coefficients A are evaluated by solving Eq. (9) and the wave forces are obtained using Eq. (10):

$$\left|\frac{F^j}{F}\right| = \frac{1}{2}\left|A^j_{-1} \pm A^j_1\right| \tag{10}$$

The subtraction of the coefficients on the right hand side gives the wave force along the x-axis and the addition of the terms gives the wave force along the y-axis. In the current study, the angle of incidence $\beta = 0$ and the waves propagate along the x-axis.

4. Results

4.1. Validation of the numerical model

The numerical model is validated by simulating the experiments carried out at the Large Wave Flume (GWK), Hannover, Germany by Mo et al. (2007). The numerically computed values for the free surface elevation around the cylinder, the water particle velocity in the numerical wave tank and the wave force on the cylinder are compared with the experimental data to confirm that the numerical model accurately calculates the wave kinematics and dynamics. The wave flume in the experiments is 309m long, 5m wide and 7m deep. A cylinder of diameter $D = 0.7$m is placed 111m from the wavemaker and strain gages are placed at the top and bottom of the cylinder in order to measure wave forces. Wave gages are placed at several locations around the cylinder to measure the time histories of the free surface elevation. Four acoustic Doppler velocimeters (ADVs) are placed at the side wall along the front line of the cylinder at various depths to measure the water particle velocities.

The numerical wave tank used in this simulation is 132m long, 5m wide and 8m high. Fifth-order Stokes waves with wave height $H = 1.2$m, wave period $T = 4.0$s, wavelength $L = 21.9$m are generated with a water depth $d = 4.76$m on a grid of $dx = 0.1$m. The grid in the numerical wave tank is $1320 \times 50 \times 80$ cells resulting in a total number of 5.28 million cells. The cylinder is placed in the center with respect to the side walls as seen in the numerical setup in Fig. (1). The diffraction parameter $D/L = 0.032$ and KC=6.1 in this case.

A net inline force acts on the cylinder due a difference in pressure in front and behind the cylinder. The calculated force on the cylinder is compared with the experimental data and a good agreement is seen in Fig. (2a). Mo et al. (2007) noted that the force measured in the experiments matched the inertial force given by the Morison formula with $C_m = 2$. So, it appears that the forces are inertia dominated, although the KC number is 6.1 in this case. A grid convergence study for the forces is carried out by repeating the simulations with grid sizes of $dx = 0.15$m and 0.2m. The force in these cases is compared with the calculated force using a grid size of $dx = 0.1$m and the experimental result. It is seen that the numerical result converges to the experimental value at a grid size of $dx = 0.1$m in Fig. (2b). Thus, the selected grid size is sufficiently small to accurately calculate the force on the cylinder.

The numerically obtained free surface elevation near the wall along the front line of the cylinder is compared with the experimental data in Fig. (3a). The amplitude at the first crest is considered the maximum amplitude of the wave elevation recorded by the gage near the wall, $\eta_{max,wall}$. The comparisons of the computed and measured free surface elevation in front, at the side and behind the cylinder are presented in Fig. (3b), (3c) and (3d) respectively. The difference in pressure in front and behind the cylinder is seen in the free surface elevation around the cylinder. The numerically obtained free surface elevation data shows a good match with the experimental measurements. The water particle velocity calculated by the numerical model is compared with the experimental measurements at 0.93m, 1.53m and 2.73m below the still water level at the side wall of the tank along the front line of the cylinder in Fig. (4). The numerical results are scaled with the numerically calculated wave celerity, $C = 5.48$m/s. The water particle velocity is expected to reduce with increasing distance from the free surface as seen in Fig. (4) with the amplitude of the velocity being the lowest in Fig. (4a) at 2.73m from the still water level. The water particle velocities calculated by the model match the values observed in the experiments very well, showing that the numerical model is able to represent the wave kinematics correctly.

4.2. Grid convergence study for wave propagation

Accurate wave generation and propagation in the numerical wave tank is verified with a grid convergence study. A two-dimensional wave tank with a length of 15m, height of 1.0m and water depth $d = 0.5$m is used. Fifth-order Stokes waves are generated with a wave height of $H = 0.1$m, a wavelength of $L = 2.0$m and wave period $T = 1.14$s. This setup of the numerical wave tank is used in the following sections to simulate the wave interaction with large cylinders. The grid convergence is carried out for the most stringent case with the highest wave steepness used in the study. The grid size dx in the wave tank is varied from 0.1m to 0.01m. The results are presented in Fig. (5). It is seen that the free surface elevation η conforms to the required value at a grid size of $dx = 0.025$m. The damping of the wave amplitude at grid sizes of 0.1m and 0.05m is seen in the figure. This is reduced as the grid size is reduced to 0.025m and the improvement in the results on further reducing the grid size is negligible. Thus, a grid size of $dx = 0.025$m is selected for the following simulations in the current study.

4.3. Wave interaction with a single large cylinder

Simulations are carried out with a cylinder of diameter $D = 0.5$m in a wave tank 15m long, 5m wide and 1m high with a water depth of $d = 0.5$m. Linear waves of height H=0.006m and 0.02m, second-order Stokes waves with H=0.06m and 0.1m, fifth-order Stokes waves with H=0.11m, 0.12m, 0.13m, 0.14m, 0.15m, 0.16m, 0.18m and 0.2m with a wavelength $L = 2$m are incident on the cylinders resulting in D/L=0.25. The KC numbers for these simulations are between 0.04 and 1.37. The resulting wave steepnesses and the incident wave frequency for the different cases are listed in Table (1). The linear and $2nd$-order Stokes waves have the same wave frequency for different incident wave heights but in the case of $5th$-order Stokes waves the wave height is included in the dispersion relation and a small decrease in the wave frequency is seen with increasing wave height. The computed inline wave force on the cylinder for $H/L = 0.003$ is compared to the analytically predicted maximum and minimum value from the MacCamy-Fuchs equation and a good agreement is seen in Fig. (6a). The computed wave force on the cylinder for different wave steepnesses is compared with the prediction from the MacCamy-Fuchs equation in Fig. (6b). It is seen that the numerical results agree with the predictions at lower wave steepnesses but the numerical results for the higher wave steepnesses are seen to be lower than the predictions from the equation. According to the MacCamy-Fuchs equation, the wave force on the cylinder increases linearly with an increase in the incident wave height H for a given cylinder diameter D. The variation of the computed force on the cylinder with increasing steepness suggests that the total force on the cylinder is reduced due to non-linear interaction of high-steepness waves with the cylinder and the diffracted waves.

The variation of the free surface elevation η in front, behind and beside the cylinder for an incident wave of low steepness $H/L = 0.003$ shows 1.72 times the incident wave crest height η_{c_i} in front of the cylinder in Fig. (7a). The phase difference in the wave elevations in front and behind the cylinder is 0.78π and 0.24π for the wave elevations in front and beside the cylinder. In the case of an incident wave with the high steepness of $H/L = 0.1$ in Fig. (7b), the evolution of wave asymmetry is apparent with the crest height $1.55\eta_{c_i}$ and the trough $0.95\eta_{c_i}$ in front of the cylinder. The phase difference between the wave elevations in front and behind the cylinder is 0.80π and 0.20π for the elevation in front and beside the cylinder. Thus, the high steepness waves move faster around the upstream half of the cylinder but slower around the downstream half of the cylinder, in comparison to the waves of low steepness. This points towards a deceleration of the water particles in the region after the upstream half of the cylinder. The waveform behind the cylinder is also highly asymmetrical, resulting in shallower troughs behind the cylinder, when a crest is incident in front of the cylinder. This increased asymmetry points towards a different pressure difference regime in the case of the high-steepness waves. As a result of the deceleration of the water particles and the asymmetry of the wave, the force acting on the cylinder due to an incident wave of high steepness is lower than the prediction from MacCamy-Fuchs equation based on linear potential theory.

4.4. Wave interaction with a pair of tandem cylinders

A set of simulations is carried out to study the wave interaction with two cylinders placed in tandem in the direction of wave propagation. Cylinders with diameter $D = 0.5$m are placed in a wave tank that is 15m long, 5m wide and 1m high with a water depth $d = 0.5$m on a grid of $dx = 0.025$m. A schematic diagram illustrating the numerical setup is given in Fig. (8). The grid is $600\times200\times40$ cells resulting in a total of 4.80 million cells in the numerical wave tank. Linear waves with wave height H=0.006m and 0.02m, second-order Stokes waves with H=0.06m and 0.1m, fifth-order Stokes waves with H=0.11m, 0.12m, 0.13m, 0.14m, 0.15m, 0.16m, 0.18m and 0.2m with a wavelength $L = 2$m are incident on the cylinders. The KC numbers in these cases range between 0.04 and 1.37. For each of the incident wave heights, centre-to-centre distance between the two cylinders, S=0.8m, 1.2m, 1.6m, 1.8m, 2.0m, 2.3m and 3.37m are simulated. The different combinations of incident wave steepness and the center-to-center distance for the 96 simulations are listed in Table (2). The cylinder directly facing the incident waves is cylinder 1 and the downstream cylinder is cylinder 2. Previous works using analytical methods (Linton and Evans (1990), McIver and Evans (1984), Malenica et al. (1999)) have shown that the wave forces on tandem cylinders are influenced by not only the incident wave height and the spacing between the cylinder, but also by the incident wave frequency. In order to maintain the focus on the effect of the incident wave height with small increments in wave steepness for different distances between the cylinder, the effect of the incident wave frequency is not analysed in this paper.

The variation of the computed inline wave force on the cylinders with center-to-center distances S for different incident wave steepnesses H/L is presented in Fig. (9). The prediction from the formula by Linton and Evans (1990) is also included for obtaining a baseline comparison. It is clearly seen that the analytical prediction matches the computed wave force closely at the lowest wave steepness of $H/L = 0.003$ for both cylinders, in Fig. (9a) and (9b). The computed wave forces show a similar form of variation for $H/L = 0.05$ as predicted by the analytical formula but with lower magnitudes in Fig. (9c) and (9d). The deviation from the predictions by the analytical formula is clear in Figs.(9e) and (9f) for the highest wave steepness simulated, $H/L = 0.1$. In addition to the amplitude of the force, the form of the variation is also different at longer distances of separation S. Cylinder 1 experiences large changes in the wave force when the center-to-center distance between the cylinders is changed. The difference between the largest force at $S = 0.8$m and the lowest force at $S = 3.37$m is 35% for $H/L = 0.003$ and $H/L = 0.05$, but about 22% for $H/L = 0.1$. The change in the center-to-center distance S strongly affects cylinder 2 at small values of $S = 0.8$m and $S = 1.2$m, with a change of 17.4% for $H/L = 0.003$, 18% for $H/L = 0.05$ and 16% for $H/L = 0.1$. Whereas, the difference in the forces at $S = 2.0$m and $S = 3.37$m is 8% for $H/L = 0.003$, 4% for $H/L = 0.05$ and 2.5% for $H/L = 0.1$. It is observed that the Bessel wave-like variation of the wave forces with the center-to-center distance is damped out with increasing incident wave steepness for both cylinders. Even though, the analytically predicted wave force on cylinder 1 matches the computed wave force at $S = 3.37$m for $H/L = 0.05$ in Fig. (9c) and $S = 2.3$m, $S = 3.37$m for $H/L = 0.1$ in Fig. (9e), the wave force variation with S is clearly different.

The variation of the wave forces on the two cylinders for different center-to-center distances S at various incident wave steepnesses H/L is presented in Fig. (10). It is seen that the wave forces on both cylinders match the analytical prediction at lower $H/L = 0.003$ and 0.01. On increasing the wave steepness, the computed wave forces gradually deviate from the analytical prediction. The computed forces are lower than the predictions from the analytical formula. The computed wave force on cylinder 1 at $S = 0.8$m for $H/L = 0.1$ is 30% lower than the analytical prediction and 35% lower on cylinder 2 (Fig. 10a). It is also observed that at a center-to-center distance of $S = 3.37m$ (Fig. 10h), the wave forces on both the cylinders are almost equal. At this point, the effect of diffraction in between the two cylinders is reduced significantly and it does not influence the wave forces on the cylinders anymore.

Wave gages are placed in front ($F1$, $F2$), behind ($B1$, $B2$), beside each of the cylinders ($C1$, $C2$) and at the midpoint between the two cylinders ($C0$) at locations shown in Fig. (11) for $H/L = 0.003$ and $H/L = 0.1$ with $S = 0.8$m. In the case of low steepness incident waves of $H/L = 0.003$, the variation of the free surface elevation is sinusoidal around both the cylinders in Figs. (12a) and (12b). It is observed that the crest height is increased in front of the cylinders due to the incident wave interaction with the cylinders ($F1$, $F2$) and due to the superposing of the incident waves and the reflected waves behind the cylinder ($B1$). The computed free surface elevations at $B1$, $F2$ and $C0$ have the same amplitude and phase, implying uniform heave motion of the water along the line joining the centers of the two cylinders.

In the case of high steepness incident waves of $H/L = 0.1$, the incident waveform is asymmetrical with shallow troughs and sharp crests in Figs. (12c) and (12d), characteristic of fifth-order Stokes waves. The waveform computed at $C1$ shows increased asymmetry compared to the incident waves. This is attributed to the interaction of the incident waves with the out of phase reflected waves from the cylinder. Wage gages $B1$, $C0$ and $F2$ show a continuously increasing crest elevation as the wave propagates away from cylinder 1 and towards cylinder 2, due to the strong diffraction regime between the two cylinders. The crest elevation then reduces at $C2$ and $B2$, as the wave propagates around cylinder 2. Also, the free surface elevations at $B1$, $C0$ and $F2$ are slightly out of phase and have different amplitudes signifying a complex wave diffraction regime in the region between the cylinders.

Several differences are observed between the interaction of low and high steepness waves with a pair of tandem cylinders. The incident high steepness fifth-order waves are asymmetrical by nature with a shallow trough and a sharp crest. This characteristic of the waves is magnified as it interacts with the large cylinders and the waveform becomes more asymmetrical. This is in contrast to the interaction of the low steepness linear waves, where the waveforms remain sinusoidal. The relative crest height η/η_{c_i} in front of the cylinders is similar for both high and low steepness waves. This is clearly seen in the case of the downstream cylinder 2, where the relative crest height in front of the cylinder looks similar in Fig. (12b) and (12d) but the waveform is highly asymmetrical for $H/L = 0.1$. Also, the free surface elevation is seen to continuously increase as the wave propagates away from cylinder 1 and towards cylinder 2. This large variation is not seen for the low steepness waves, where the free surface elevation behind cylinder 1, in front of cylinder 2 and at the midpoint between the two cylinders is seen to be the same. A uniform heave motion of the water is observed along the line joining the centers of the cylinders for low steepness waves and this is absent in the case of high steepness waves. These changes seen in the wave interaction with a pair of tandem cylinders for incident waves of low and high steepness result in different flow regimes in the two cases. This justifies the large deviation observed in the calculated wave force compared to the analytical predictions for high wave steepnesses.

In order to obtain further clarity on the wave field around the two tandem cylinders with $S = 0.8$m, the diffraction patterns around the cylinders for $H/L = 0.003$ and $H/L = 0.1$ are studied. The free surface elevation around the cylinders in the numerical wave tank for $H/L = 0.003$ over one wave period is presented in Fig. (13). The increase in the free surface elevation when the crest is incident on cylinder 1 is seen in Fig. (13a) and Fig. (13b) shows the change in the wavefront due to wave diffraction around cylinder 1. The decrease in the free surface elevation as the wave travels around the upstream half of cylinder 1 is seen in Fig. (13c). Figure (13d) shows the increase in the free surface elevation as the crest is incident on cylinder 2 and reduced free surface elevations are seen in behind cylinder 2 in Figs. (13e) and (13f). The region between the two cylinders with equal free surface elevation contours in all the figures is the region with the uniform heave motion of the free surface.

Figure (14) shows the variation of the free surface elevation around the two tandem cylinders with $S = 0.8$m for $H/L = 0.1$ over one wave period. The increase in the free surface elevation in front of the cylinder and the formation of distinct reflected waves is seen in Figs. (14a) and (14b). The incident and reflected waves meet behind cylinder 1 in Fig. (14c) and the intersection of two semi-circular waves is seen. The constructive interference of the two semi-circular waves in the region between the two cylinders leading to a continuous increase in the free surface elevation around the line joining the centers of the cylinders in Fig. (14d). The resulting large free surface elevation in front of cylinder 2 is also seen in the figure. Figure (14e) shows the reflected waves in between the cylinders over the trough of the incident wave. The circular diffracted waves formed in the wave tank around the two cylinders is seen in Fig. (14f).

The free surface elevation contours around the tandem cylinders in the simulations with a low wave steepness of $H/L = 0.003$ and a high wave steepness of $H/L = 0.1$ show that the wave regime is different in the two cases. The incident straight wavefronts transform to a bent wavefront due to diffraction in the case of low steepness waves. In the case of the high steepness waves, formation of several semi-circular diffracted wavefronts are seen in addition to the bending of the incident wavefront. A uniform heave motion of the free surface is seen for the waves of low steepness in the region between the two cylinders. In the case of the high steepness waves, distinct semi-circular diffracted waves interfere constructively in the region between the two cylinders. The large free surface elevation is concentrated around the line joining the centers of the two cylinders. It is seen in the numerical results that the interaction of high steepness waves is different from low steepness waves due to the strong diffraction pattern and the transformation of the high steepness waves. The non-linear wave interaction in the case of high steepness waves are not accounted for in the analytical formulae based on potential theory. This results in the difference between the computed wave forces on the cylinders compared to those predicted by the analytical formulae.

5. Conclusions

The calculation of wave forces on a single cylinder using the open source CFD model REEF3D is validated by comparison of experimental data for wave forces, wave elevation around the cylinder and water particle velocity with the computed results from the numerical wave tank. Simulations are carried out to study the wave interaction with a large cylinder for different wave steepnesses. The numerically calculated wave forces match the predictions by MacCamy-Fuchs equation for low wave steepnesses. Whereas for higher wave steepnesses, the computed wave forces are lower than the predictions by the equation. The wave elevation around the cylinder is investigated and the evolution of an asymmetrical waveform is seen in the case of high steepness waves, whereas low steepness waves maintain their symmetrical sinusoidal form. The difference in the wave phase in front, beside and behind the cylinder suggest a deceleration of water particles around the downstream half of the cylinder in the case of high steepness waves.

Further, simulations with a pair of large tandem cylinders are carried out with different incident wave steepnesses and center-to-center distances between the two cylinders. The computed wave forces are compared with the predictions from an analytical formula based on potential theory. It is observed that the computed wave forces match the predicted wave forces for lower wave steepnesses. The computed wave forces are lower than the analytically predicted wave forces for higher wave steepness, with about a 35% lower force for the highest wave steepness simulated in the study. The analytical formulae predict a linear increase in the wave force with an increase in the incident wave height, for a given cylinder diameter and incident wavelength. The numerical results show that due to the wave transformation and the resulting asymmetrical nature of the higher steepness waves, the computed wave forces on the cylinders from these waves are lower than the predictions based on potential theory. The predictions from the CFD model at the scales considered in these studies is good and provides insight into the interaction between two relatively closely spaced cylinders. In the case of longer arrays of cylinders additional resonant effects such as wave near-trapping can occur, which have not been studied int his paper.

The diffraction patterns around tandem cylinders at different wave steepnesses and the wave elevation around the tandem cylinders are also studied. The evolution of semi-circular diffracted waves are seen in the case of high steepness waves, which meet on the downstream side of the first cylinder. Whereas, in the case of low steepness waves, the wavefront is only bent as a result of wave diffraction. A uniform heave motion of the free surface elevation is observed in the region in between the cylinders in the case of low steepness waves. The complex diffraction regime in the case of high steepness with clearly formed semi-circular diffracted waves results in an increasing free surface elevation as the wave crest propagates away from the upstream cylinder and towards the downstream cylinder.

Thus, clear differences are seen between the interaction of low and high steepness waves with large cylinders. In the case of a single large cylinder, the asymmetry of the steep incident waves results in a different diffraction regime, which results in lower forces on the cylinders than predicted by linear potential theory. For a pair of tandem cylinders, the center-to-center-distance between the cylinders contributes to further change the diffraction regime, in addition to the effects due to wave asymmetry. The evolution of distinct semi-circular reflected waves around the cylinders in the case of high incident wave steepness has a consequence on objects close to the cylinders. The current results show a smooth deviation from the linear results as the incident wave steepness is increased. Further work is needed to determine the transition of the wave force regime from non-breaking wave forces where the wave forces vary at a frequency similar to the incident wave to breaking wave forces which are impulsive in nature with a sharp peak over a period much shorter than the incident wave period. Application of the numerical model to determine random wave forces can also be explored.

Acknowledgements

This study has been carried out under the OWCBW project (No. 217622/E20) and the authors are grateful to the grants provided by the Research Council of Norway. This research was supported in part with computational resources at the Norwegian University of Science and Technology (NTNU) provided by The Norwegian Metacenter for Computational Science (NOTUR, Project No. NN2620K), http://www.notur.no.

Alagan Chella, M., Bihs, H., Myrhaug, D., Muskulus, M., 2015. Breaking characteristics and geometric properties of spilling breakers over slopes. Coastal Engineering 95, 4–19.

Berthelsen, P.A., Faltinsen, O.M., 2008. A local directional ghost cell approach for incompressible viscous flow problems with irregular boundaries. Journal of Computational Physics 227, 4354–4397.

Boccotti, P., Arena, F., Fiamma, V., Barbaro, G., 2012. Field experiment on random wave forces acting on vertical cylinders. Probabilistic Engineering Mechanics 28, 39–51.

Boccotti, P., Arena, F., Fiamma, V., Romolo, A., 2013. Two small-scale field experiments on the effectiveness of morison's equation. Ocean Engineering 57, 141–149.

Boo, S.Y., 2002. Linear and nonlinear irregular waves and forces in a numerical wave tank. Ocean Engineering 29, 475 – 493.

Chakrabarti, S.K., Tam, W.A., 1973. Gross and local wave loads on a large vertical cylinder – theory and experiment, in: Proc., Offshore Technology Conference, Dallas, USA.

Chorin, A., 1968. Numerical solution of the Navier-Stokes equations. Mathematics of Computation 22, 745–762.

Durbin, P.A., 2009. Limiters and wall treatments in applied turbulence modeling. Fluid Dynamics Research 41, 1–18.

Ferrant, P., 1995. Time domain computation of nonlinear diffraction loads upon three dimensional floating bodies, in: Proc., $5th$ International Offshore and Polar Engineering Conference, The Hague, The Netherlands.

Isaacson, M., 1979. Wave induced forces in the diffraction regime. Pitman Advanced Publishing Program.

Jacobsen, N.G., Fuhrman, D.R., Fredsøe, J., 2011. A wave generation toolbox for the open-source CFD library: OpenFOAM. International Journal for Numerical Methods in Fluids 70, 1073–1088.

Jiang, G.S., Peng, D., 2000. Weighted ENO schemes for Hamilton-Jacobi equations. SIAM Journal on Scientific Computing 21, 2126–2143.

Jiang, G.S., Shu, C.W., 1996. Efficient implementation of weighted ENO schemes. Journal of Computational Physics 126, 202–228.

Larsen, J., Dancy, H., 1983. Open boundaries in short wave simulations - a new approach. Coastal Engineering 7, 285–297.

Lighthill, J., 1979. Waves and hydrodynamic loading, in: Proc., $2nd$ International Conference on Behaviour of Offshore Structures, London, England.

Linton, C.M., Evans, D.V., 1990. The interaction of waves with arrays of vertical circular cylinders. Journal of Fluid Mechanics 215, 549–569.

MacCamy, R., Fuchs, R., 1954. Wave forces on piles: A diffraction theory. University of California, Dept. of Engineering.

Malenica, S., Taylor, R.E., Huang, J.B., 1999. Second-order water wave diffraction by an array of vertical cylinders. Journal of Fluid Mechanics 390, 349–373.

McIver, P., Evans, D.V., 1984. Approximation of wave forces on cylinder arrays. Applied Ocean Research 6, 101–107.

Mo, W., Irschik, K., Oumeraci, H., Liu, P., 2007. A 3D numerical model for computing non-breaking wave forces on slender piles. Journal of Engineering Mathematics 58, 19–30.

Molin, B., 1979. Second order diffraction loads upon three-dimensional bodies. Applied Ocean Research 1, 197–202.

Naot, D., Rodi, W., 1982. Calculation of secondary currents in channel flow. Journal of the Hydraulic Division, ASCE 108, 948–968.

Ohkusu, M., 1974. Hydrodynamic forces on multiple cylinders in waves, in: Proc., International Symposium on Dynamics of Marine Vehicles and Structures in Waves, London, England, pp. 107–112.

Osher, S., Sethian, J.A., 1988. Fronts propagating with curvature- dependent speed: algorithms based on Hamilton-Jacobi formulations. Journal of Computational Physics 79, 12–49.

Peng, D., Merriman, B., Osher, S., Zhao, H., Kang, M., 1999. A PDE-based fast local level set method. Journal of Computational Physics 155, 410–438.

Shu, C.W., Osher, S., 1988. Efficient implementation of essentially non-oscillatory shock capturing schemes. Journal of Computational Physics 77, 439–471.

Song, H., Tao, L., Chakrabarti, S., 2010. Modelling of water wave interaction with multiple cylinders of arbitrary shape. Journal of Computational Physics 229, 1498–1513.

Spring, B., Monkmeyer, P.L., 1974. Interaction of plane waves with vertical cylinders, in: Proc., International Conference on Coastal Engineering, ASCE, Copenhagen, pp. 1828–1847.

Twersky, V., 1952. Multiple scattering of radiation by an arbitrary configuration of parallel cylinders. Journal of Acoustical Society of America 24, 42–46.

van der Vorst, H., 1992. BiCGStab: A fast and smoothly converging variant of Bi-CG for the solution of nonsymmetric linear systems. SIAM Journal on Scientific and Statistical Computing 13, 631–644.

Wilcox, D.C., 1994. Turbulence modeling for CFD. DCW Industries Inc., La Canada, California.

L [m]	H/L											
	linear waves		$2nd$-order Stokes		$5th$-order Stokes							
2.0	0.003	0.01	0.03	0.05	0.055	0.06	0.065	0.07	0.075	0.08	0.09	0.10
f [Hz]	0.846	0.846	0.846	0.846	0.862	0.865	0.868	0.872	0.876	0.880	0.889	0.899

Table 1: Combination of parameters for simulations with a single large cylinder of diameter $D = 0.5$m in a water depth of $d = 0.5$m

S [m]	H/L											
	linear waves		$2nd$-order Stokes		$5th$-order Stokes							
0.8	0.003	0.01	0.03	0.05	0.055	0.06	0.065	0.07	0.075	0.08	0.09	0.10
1.2	0.003	0.01	0.03	0.05	0.055	0.06	0.065	0.07	0.075	0.08	0.09	0.10
1.6	$\vdots$	$\vdots$	$\vdots$	$\vdots$	$\vdots$	$\vdots$	$\vdots$	$\vdots$	$\vdots$	$\vdots$	$\vdots$	$\vdots$
1.8	$\vdots$	$\vdots$	$\vdots$	$\vdots$	$\vdots$	$\vdots$	$\vdots$	$\vdots$	$\vdots$	$\vdots$	$\vdots$	$\vdots$
2.0	$\vdots$	$\vdots$	$\vdots$	$\vdots$	$\vdots$	$\vdots$	$\vdots$	$\vdots$	$\vdots$	$\vdots$	$\vdots$	$\vdots$
2.3	$\vdots$	$\vdots$	$\vdots$	$\vdots$	$\vdots$	$\vdots$	$\vdots$	$\vdots$	$\vdots$	$\vdots$	$\vdots$	$\vdots$
2.8	$\vdots$	$\vdots$	$\vdots$	$\vdots$	$\vdots$	$\vdots$	$\vdots$	$\vdots$	$\vdots$	$\vdots$	$\vdots$	$\vdots$
3.37	0.003	0.01	0.03	0.05	0.055	0.06	0.065	0.07	0.075	0.08	0.09	0.10

Table 2: Combination of parameters for simulations with two tandem large cylinders with diameter $D = 0.5$m, incident wavelength $L = 2.0$m in a water depth $d = 0.5$m

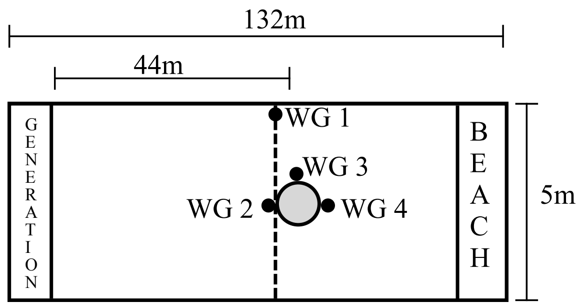

Figure 1: Numerical setup used for validation of the model

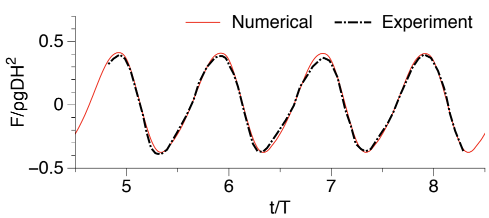

(a) wave force on a single circular cylinder

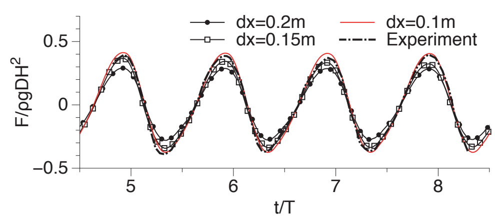

(b) convergence study for wave force calculation

Figure 2: Comparison of experimental and numerical results for the inline wave force on the cylinder

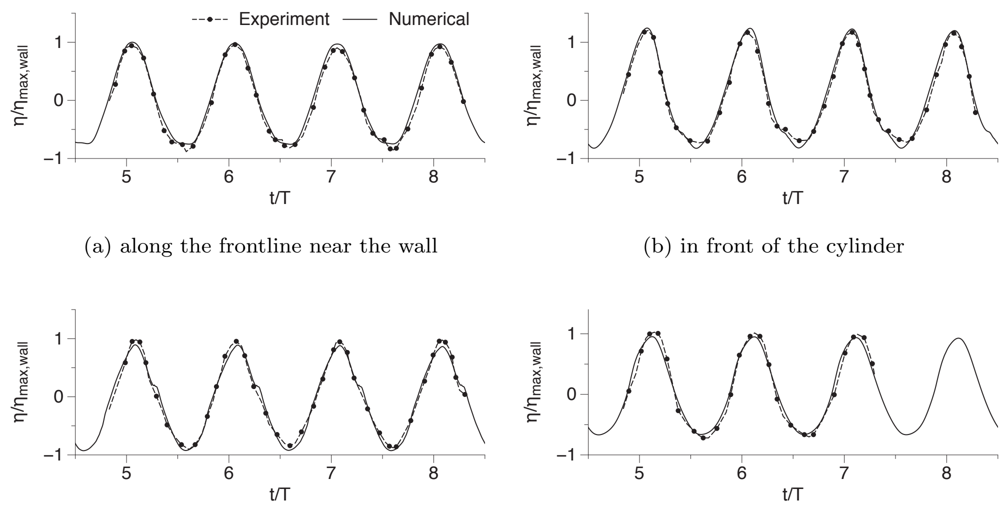

(a) along the frontline near the wall

(b) in front of the cylinder

(c) behind the cylinder

(d) beside the cylinder

Figure 3: Comparison of experimental and numerical results for free surface elevations around the cylinder

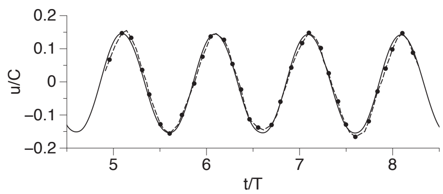

(a) $z = -0.93\text{m}$

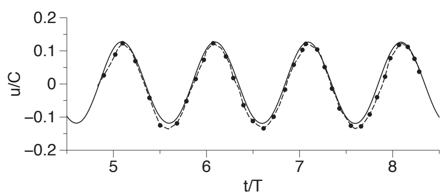

(b) $z = -1.53\text{m}$

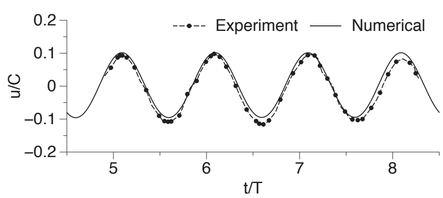

(c) $z = -2.73\text{m}$

Figure 4: Comparison of experimental and numerical results for wave particle velocity in the wave tank

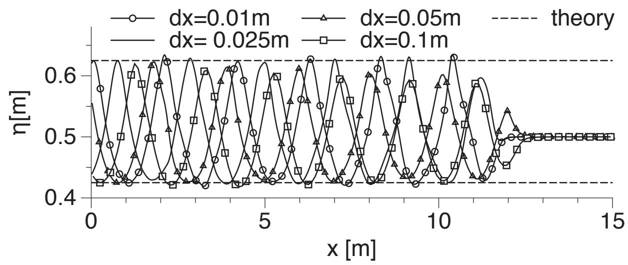

Figure 5: Grid convergence study for wave propagation

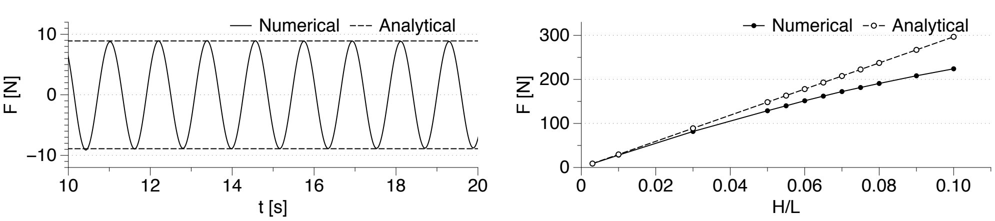

(a) $H = 0.006$m

(b) wave force for different incident wave steepnesses

Figure 6: Comparison of analytical and numerical results for the inline wave force on a single large cylinder

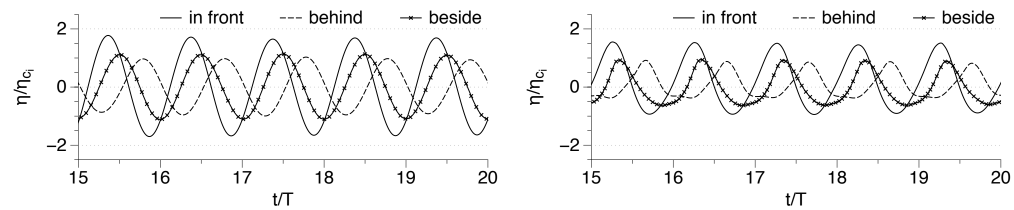

(a) $H/L = 0.003$ (b) $H/L = 0.1$

Figure 7: Relative free surface elevations around the single cylinder for incident waves of low and high steepness

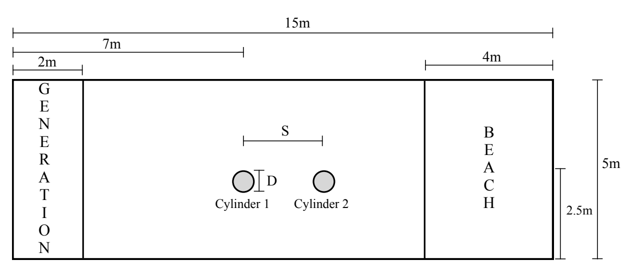

Figure 8: Schematic diagram of the setup used for the simulations with two tandem cylinders

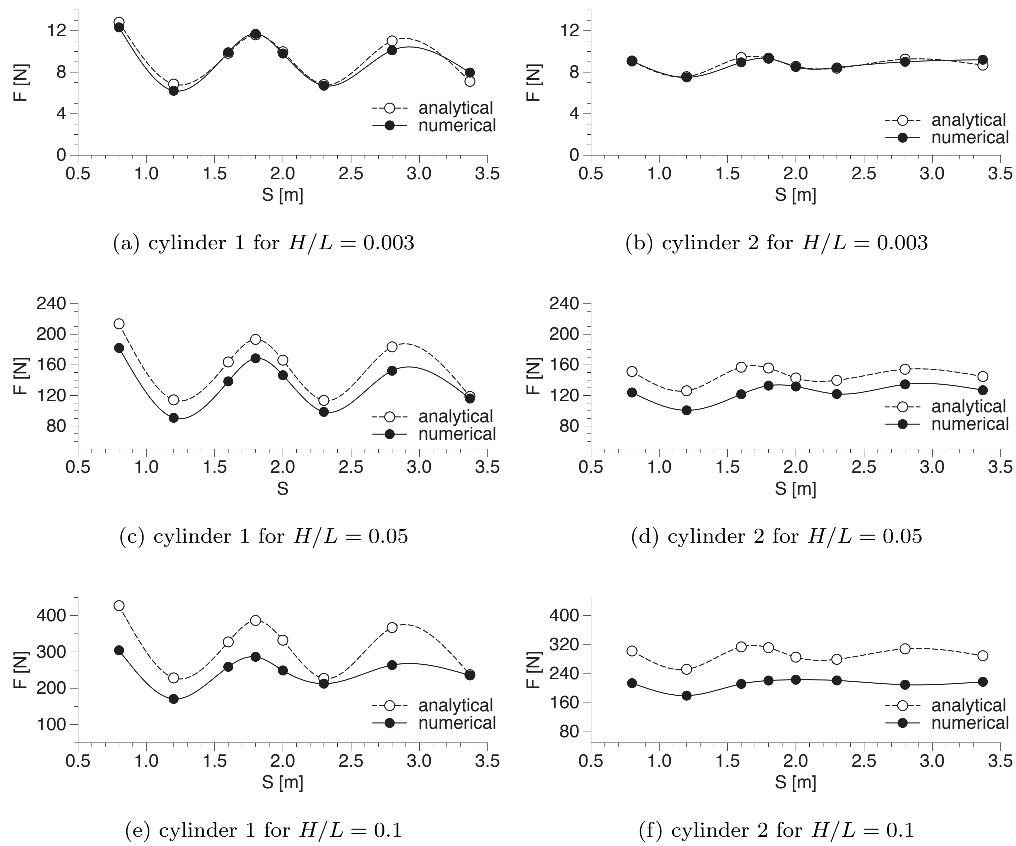

(a) cylinder 1 for $H/L = 0.003$

(b) cylinder 2 for $H/L = 0.003$

(c) cylinder 1 for $H/L = 0.05$

(d) cylinder 2 for $H/L = 0.05$

(e) cylinder 1 for $H/L = 0.1$

(f) cylinder 2 for $H/L = 0.1$

Figure 9: Variation of the inline wave forces on tandem cylinders with center-to-center distance for different wave steepnesses

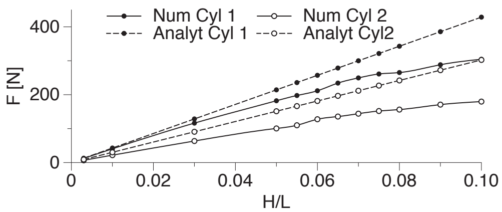

(a) $S = 0.8\text{m}$

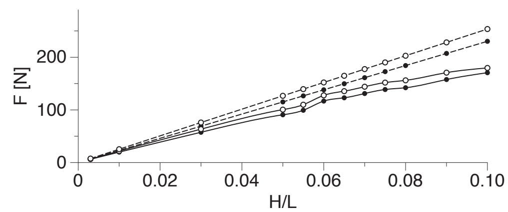

(b) $S = 1.2\text{m}$

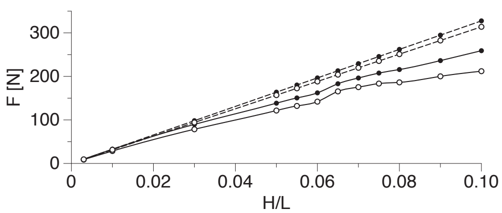

(c) $S = 1.6\text{m}$

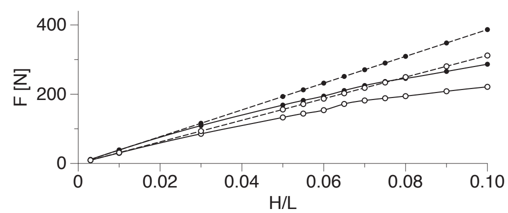

(d) $S = 1.8\text{m}$

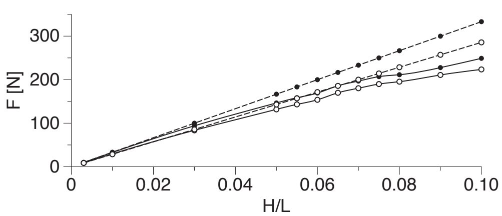

(e) $S = 2.0\text{m}$

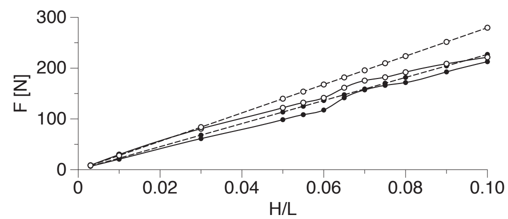

(f) $S = 2.3\text{m}$

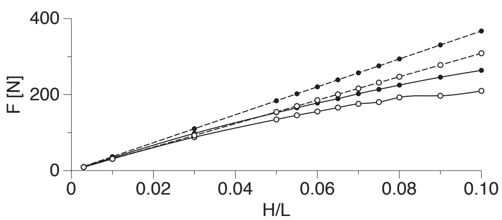

(g) $S = 2.8\text{m}$

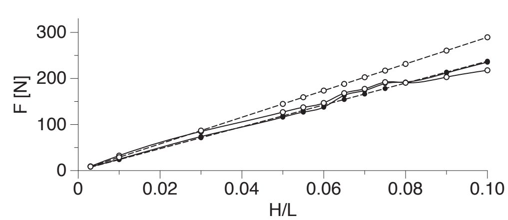

(h) $S = 3.37\text{m}$

Figure 10: Variation of the inline wave forces on tandem cylinders with wave steepness for different center-to-center distances

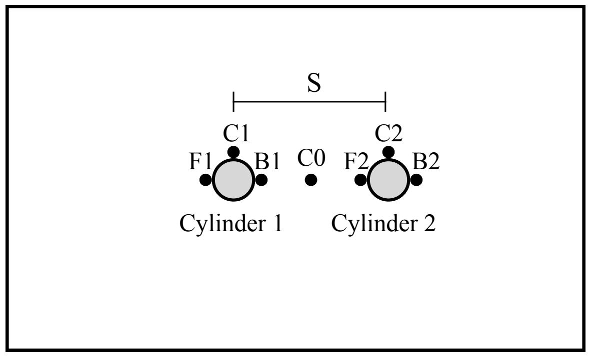

Figure 11: Schematic diagram of the domain around the two tandem cylinders showing wave gage locations

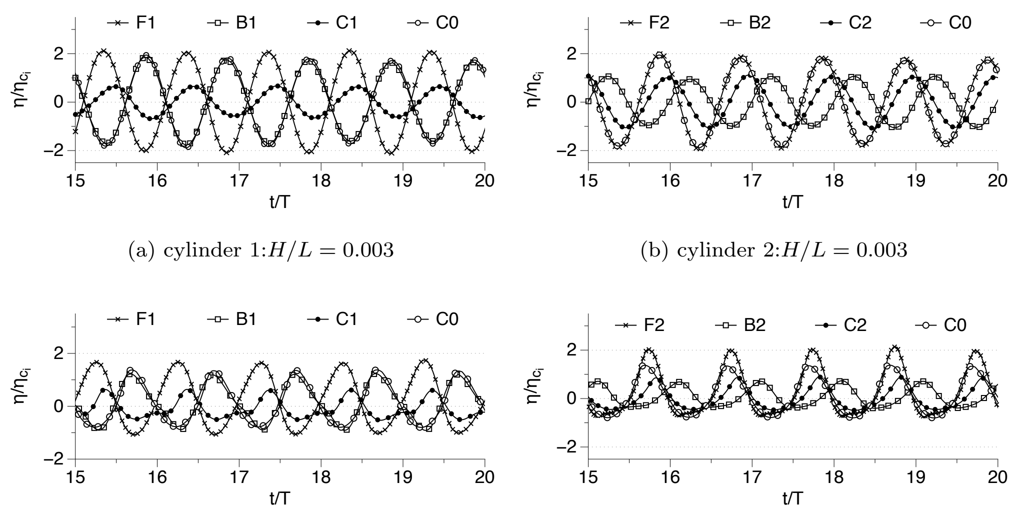

(a) cylinder 1:$H/L = 0.003$

(b) cylinder 2:$H/L = 0.003$

(c) cylinder 1:$H/L = 0.1$

(d) cylinder 2:$H/L = 0.1$

Figure 12: Relative free surface elevations around two cylinders placed in tandem with $S =$ 0.8m for incident waves of low and high steepnesses

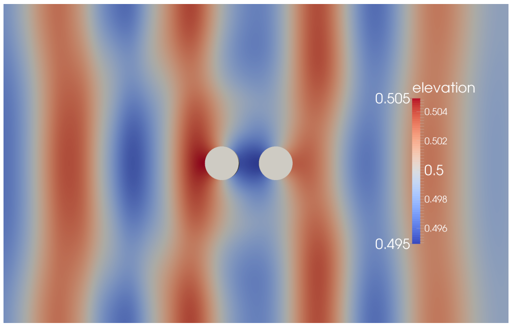

(a) t/T=32.2

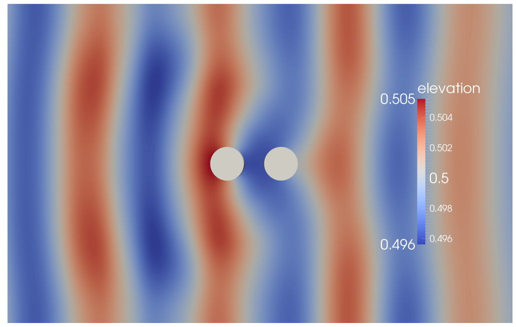

(b) t/T=32.4

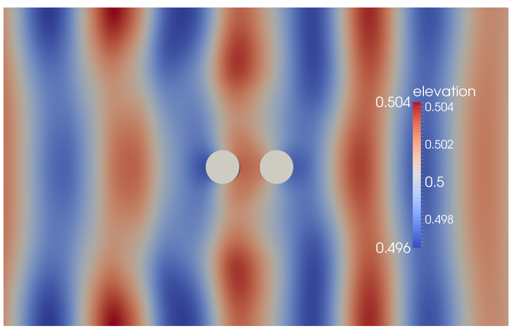

(c) t/T=32.6

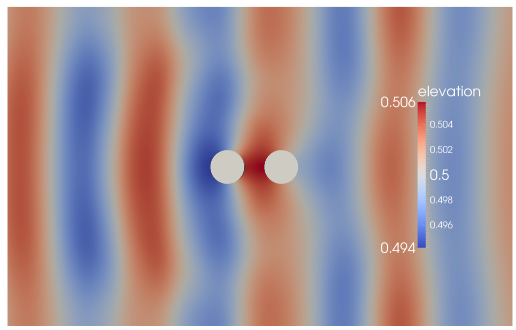

(d) t/T=32.8

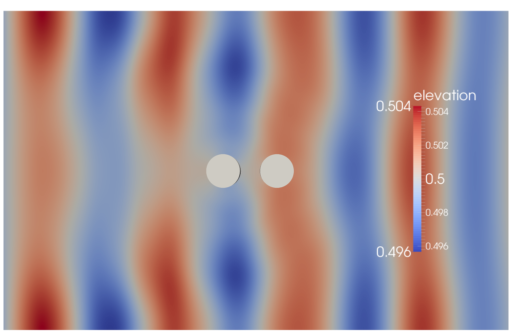

(e) t/T=33.0

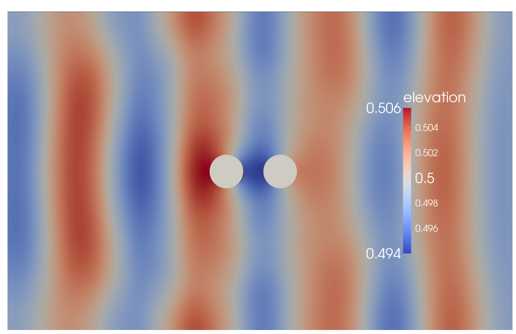

(f) t/T=33.2

Figure 13: Free surface elevation in a part of the domain around the cylinders with $S = 0.8$m for $H/L = 0.003$

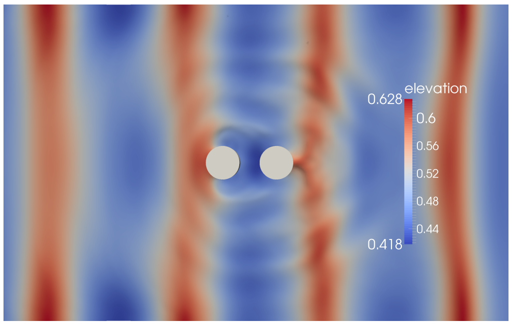

(a) t/T=32.2

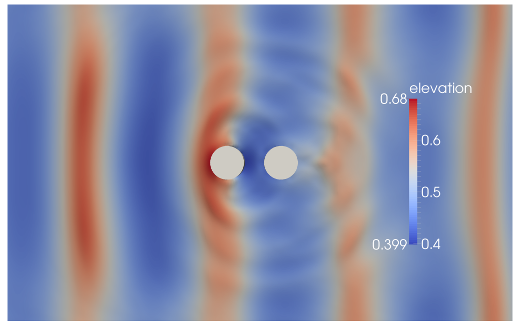

(b) t/T=32.4

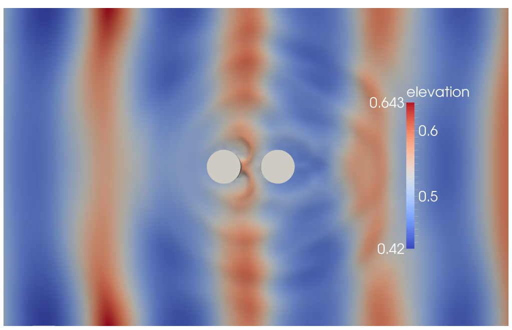

(c) t/T=32.6

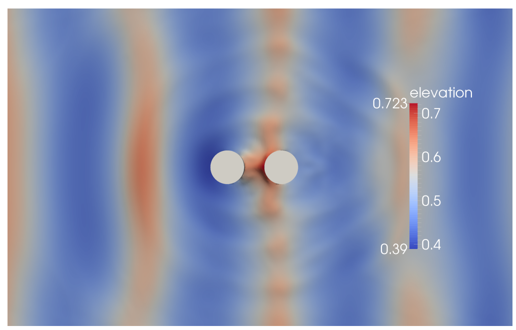

(d) t/T=32.8

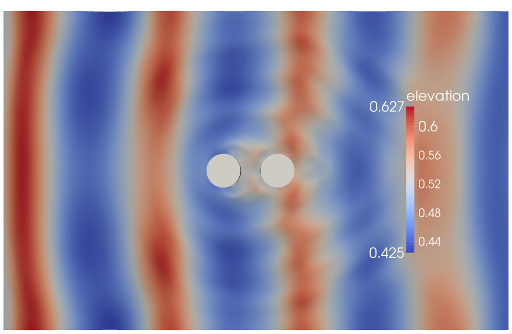

(e) t/T=33.0

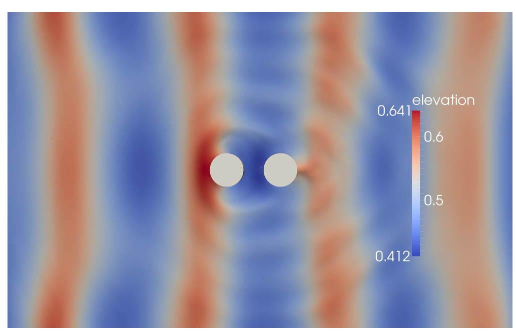

(f) t/T=33.2

Figure 14: Free surface elevation in a part of the domain around the cylinders with $S = 0.8\text{m}$ for $H/L = 0.1$